Environmental Science & Technology

Article

pubs.acs.org/est

CO_2 Hydrate Nucleation Kinetics Enhanced by an Organo-Mineral Complex Formed at the Montmorillonite−Water Interface

Daeseung Kyung,[†] Hyung-Kyu Lim,[‡] Hyungjun Kim,[‡] and Woojin Lee*,[†]

[†]Department of Civil and Environmental Engineering, Korea Advanced Institute of Science and Technology (KAIST), 291 Daehak-ro, Yuseong-gu, Daejeon 305-701, Korea

[‡]Graduate School of EEWS (Energy, Environment, Water and Sustainability), Korea Advanced Institute of Science and Technology (KAIST), 291 Daehak-ro, Yuseong-gu, Daejeon 305-701, Korea

Supporting Information

ABSTRACT: In this study, we investigated experimentally and computationally the effect of organo-mineral complexes on the nucleation kinetics of CO_2 hydrate. These complexes formed via adsorption of zwitter-ionic glycine (Gly-zw) onto the surface of sodium montmorillonite (Na-MMT). The electrostatic attraction between the $-NH_3^+$ group of Gly-zw, and the negatively charged Na-MMT surface, provides the thermodynamic driving force for the organo-mineral complexation. We suggest that the complexation of Gly-zw on the Na-MMT surface accelerates CO_2 hydrate nucleation kinetics by increasing the mineral−water interfacial area (thus increasing the number of effective hydrate-nucleation sites), and also by suppressing the thermal fluctuation of solvated Na^+ (a well-known hydrate formation inhibitor) in the vicinity of the mineral surface by coordinating with the $-COO^-$ groups of Gly-zw. We further confirmed that the local density of hydrate-forming molecules (i.e., reactants of CO_2 and water) at the mineral surface (regardless of the presence of Gly-zw) becomes greater than that of bulk phase. This is expected to promote the hydrate nucleation kinetics at the surface. Our study sheds new light on CO_2 hydrate nucleation kinetics in heterogeneous marine environments, and could provide knowledge fundamental to successful CO_2 sequestration under seabed sediments.

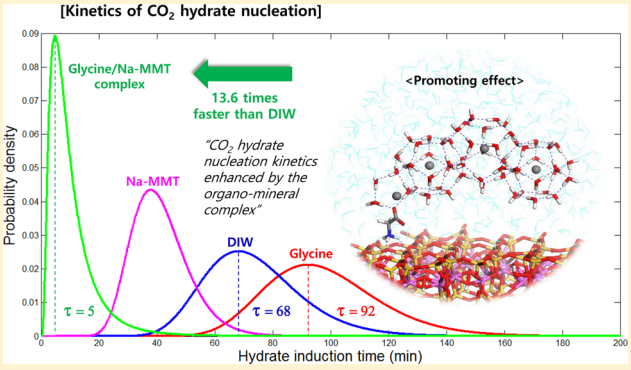

INTRODUCTION

Gas hydrates are nonstoichiometric crystalline guest−host structures in which small molecules such as CO_2 and CH_4 are trapped inside hydrogen-bonded water cages, consisting mostly of five- and six-member rings formed under high pressure and low temperature.[1,2] The ratio of water to CO_2 molecules in CO_2 hydrate has been experimentally determined to be in the range from 5.82 to 7.8. This means that 1 m^3 of CO_2 hydrate could contain 120−162 m^3 of gaseous CO_2 under hydrate-forming conditions.[3] This high storage capacity has stimulated scientists to study the formation kinetics (kinetics of nucleation and growth), phase equilibrium, and dissolution rates of these hydrates for the development of CO_2 sequestration technology.[4−9] It is anticipated that the CO_2 sequestration technology could provide a solution to an impending environmental issue, global climate change, caused by increasing anthropogenic CO_2 emissions.[4,10] It has been reported that formation of CO_2 hydrates in deep-sea sediments (>3000 m deep) during offshore CO_2 injection could prevent buoyant liquid CO_2 leakage from the sites by formation of a hydrate cap.[11,12] The hydrate cap could be stably maintained without its dissociation and dissolution in equilibrium conditions with its surroundings, i.e., it needs to be in contact with marine environment saturated by CO_2 at high pressure and low temperature for stability.[8,9] At some locations, it might be possible to simultaneously recover methane from existing gas hydrate deposits by CH_4−CO_2 replacement involving the stable gas hydrate structure.[13−15] Although dissolution of CO_2 hydrates caused by difference of chemical potential between the hydrates and seawater or pore waters (usually under-saturated with respect to CO_2) has been considered one limitation for the technology, CO_2 hydrate formation in CO_2-rich seawater (e.g., the Okinawa trough) and isolation of CO_2 hydrates from seawater with hydrocarbon films, surfactants, microbial layers, or sediments might significantly prevent CO_2 hydrate dissolution.[8,16]

To explore the potential application of CO_2 hydrates for offshore sequestration of CO_2, basic knowledge of CO_2 hydrate formation kinetics under the environmental conditions within marine sediments should be understood, along with knowledge of the phase equilibrium and dissolution of CO_2 hydrate. In

Received: June 30, 2014
Revised: December 20, 2014
Accepted: December 22, 2014
Published: December 22, 2014

DOI: 10.1021/es504450x
Environ. Sci. Technol. 2015, 49, 1197−1205

particular, accelerating hydrate formation at CO_2 storage sites is directly related to successful CO_2 sequestration. This is because the complete extension of the CO_2 hydrate layer to cap the CO_2 reservoir should be achieved faster than the rate of liquid CO_2 migration (~12.5 cm/s)[17] to prevent leakage after CO_2 injection.[18,19] Therefore, the search for proper storage sites must include those with the environmental conditions most favorable for rapid hydrate formation.

There has been research reporting that actual marine sediments (e.g., Ulleung Basin sediments in South Korea) containing high contents of organic matter (e.g., lignins, humic substances, and compounds with amide and amine groups) can significantly promote the CO_2 hydrate formation.[5,6] It has been revealed that CO_2 hydrate nucleation kinetics is significantly dependent on the characteristics of solid surfaces (e.g., surface charge, surface area, mineral type) of the sediments.[18,19] Some reactive sites on the clay mineral surfaces are involved in facilitating CO_2 hydrate crystallization by providing a well-ordered hydrate lattice and/or nucleation sites.[18,19] Organic matter associating with water molecules and chemical species on mineral surfaces, could affect the arrangement of structured or ordered water clusters, which might lead to enhanced CO_2 hydrate nucleation kinetics.[5,20]

It is known that most CO_2 hydrates can form in the pore space of marine sediments during the offshore CO_2 injection.[21] In addition, measurable concentrations (0.87−6.92 mmol/L) of dissolved free amino acids have been found in the pore water of natural marine sediments. This is due to their assimilation and production by microbial activities in the water/sediment interface and subsequent accumulation.[22−24] Therefore, high concentrations of dissolved amino acids in the pore water could form organo-mineral complexes via interactions of amino acids with mineral surfaces in the marine sediments and they could significantly influence the formation of CO_2 hydrate. However, no significant research to investigate the effect of organo-mineral complexes in the marine sediments on the nucleation kinetics of CO_2 hydrate has been conducted to date, nor is its reaction mechanism under relevant environmental conditions well-understood at this time.

In this work, we investigated the effect of organo-mineral complexes at a mineral−water interface, on CO_2 hydrate nucleation kinetics, by measuring the hydrate induction time. In addition, we performed quantum mechanical (QM) calculations and molecular dynamics (MD) simulations in systems with similar experimental conditions to extract detailed information about organo-mineral complexation and its effect on CO_2 hydrate nucleation kinetics on a molecular level.[25−28] Glycine, the amino acid with the simplest structure, was chosen for this study due to its ubiquitous occurrence in marine sediments and pore water[23] and usefulness for computer simulations. Sodium montmorillonite (Na-MMT) was selected as the representative clay mineral because it is frequently found in marine sediments in areas of specific interest, such as those holding gas hydrate deposits.[29]

METHODOLOGY

Chemicals and Sample Preparation. The hydrate-forming gas was commercial 99.9% compressed CO_2 (Sam-O Gas Co., Korea). Glycine, NaCl, and Na-MMT were purchased from the Sigma-Aldrich, Junsei, and Clay Minerals Society, respectively. The chemicals were used without any further purification. NaCl was dissolved in deionized water (DIW, 18 MΩ·cm) to prepare NaCl solution (3.5% w/w). Glycine was added to DIW or NaCl solution to prepare 100 mg/L glycine solution gravimetrically, with and without NaCl. Different concentrations of glycine solution (50, 200, 500, and 1000 mg/L) was also prepared by dissolving an exact amount of glycine in DIW. Na-MMT (0.4 g) was added to 30 mL of DIW, NaCl solution, or glycine solutions with and without NaCl to prepare the solid or organo-mineral suspensions, and then continuously mixed at 200 rpm until the measured pH did not vary by ±0.02 pH units over 5 min.

Experimental Setup. The CO_2 hydrate nucleation kinetics tests were conducted using an experimental setup designed for the formation of CO_2 hydrates[18,19] (Figure S1, Supporting Information). A cylindrical 304 stainless steel, pressurized-vessel (50 mL) reactor with two, tempered sight-ports on opposite sides, allowed visual observation during the hydrate formation experiments. A mixture of ethylene glycol and distilled water (v/v = 1:1) was used as a cooling-bath liquid. The pressure of the vessel was controlled by a pressure regulator (Crown, pressure gauge limit: 2500 bar) in the ranges of 0−30 bar, and a gas heater (Crown, maximum heating temperature: 333 K) was also used to provide constant and stable gas pressure in the vessel. The temperature and pressure sensors were connected to a data acquisition unit (Agilent 34970A) with a response time of 20s, to monitor CO_2 hydrate induction times.

Experimental Procedure. To simulate the formation of CO_2 hydrate in a natural gas hydrate forming environment, experiments were conducted under isothermal and isobaric conditions. A prepared sample (30 mL) of (1) DIW control, (2) DIW with glycine (D-G), (3) DIW with Na-MMT (D-M), (4) DIW with both glycine and Na-MMT (D-G-M), (5) NaCl solution with Na-MMT (N-M), or (6) NaCl solution with both glycine and Na-MMT (N-G-M) was poured into the hydrate-forming reaction vessel. Then the vessel was immersed in a cooling-bath to keep the temperature constant at 273.4 K during the experiments. After temperature equilibration of the reaction vessel for 30 min, the vessel was pumped down to a vacuum, then purged using gaseous CO_2 to remove air in the headspace of the reaction vessel and its suspension. The vessel was allowed to stand until its temperature and pressure reached equilibrium again (~10 min). CO_2 gas was then injected into the vessel until its pressure reached the desired experimental pressure (30 bar) and then was continuously supplemented to keep the pressure constant during the experiment. The changes of temperature and pressure in the vessel were monitored until the CO_2 hydrate was formed and fully developed (no further detection of pressure decrease by CO_2 hydrate formation). The time interval from the onset of CO_2 pressurization to detection of a sharp temperature increase resulting from hydrate nucleation (exothermic reaction) was regarded as the CO_2 hydrate induction time. Visual observation was performed to double-check CO_2 hydrate formation in the reaction vessel. Each experimental run (200 min) was repeated 20 times under the same conditions (Tables S1 and S2, Supporting Information) to obtain statistical hydrate induction time data. This was deemed necessary due to the stochastic nature of hydrate nucleation involving a complex interaction between host and guest molecules.[6]

Stochastic Data Analysis. Commercial statistical software, Crystal Ball v. 11.1 (Oracle) was used to generate histograms and to fit probability distributions based on experimental data. All of the experimental data were fitted by log-normal distribution because it is known that the lifetime distribution

DOI: 10.1021/es504450x
Environ. Sci. Technol. 2015, 49, 1197−1205

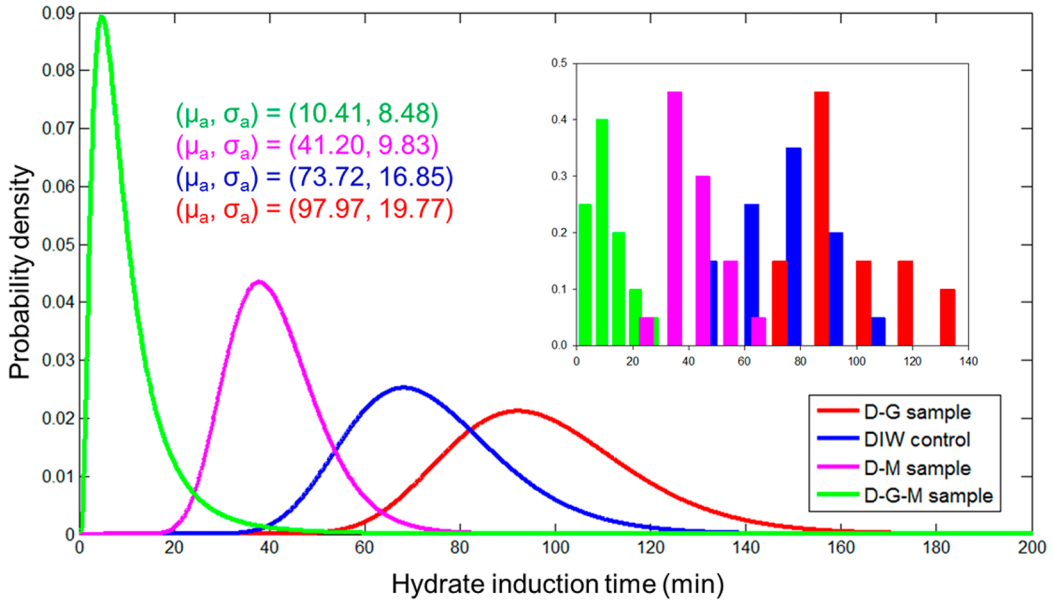

Figure 1. Relative-frequency histograms (inset) and variation of log-normal-fits of measured CO_2 hydrate induction times under different experimental conditions in DIW. Arithmetic mean (μ_a) and standard deviation (σ_a) of log-normal distribution of CO_2 hydrate induction times decrease in the following order: D-G, DIW, D-M, and D-G-M.

of prehydrate structure, and hydrate induction time, can be described by log-normal fitting.[6,30] To check the *p*-values of the fitted distribution, goodness-of-fit tests were performed with the Anderson–Darling (A-D) and Kolmogorov–Smirnov (K-S) tests.[6] When *p*-values based on the tests exceeded 0.05, a "suitability of log-normal probability distribution function" was confirmed. The arithmetic mean (μ_a) and standard deviation (SD, σ_a) of the log-normal distribution were calculated by $e^{\mu+(\sigma^2/2)}$ and $(e^{2(\mu+\sigma^2)} - e^{2\mu+\sigma^2})^{1/2}$, respectively. The parameters were used to investigate the effect of glycine, Na-MMT, and their interaction, on hydrate induction time, and on its consistency.

Quantum Mechanical Simulation. Density functional theory (DFT) is based on the accurate quantum mechanics calculations on large systems, providing ground state total energies of reactants, intermediates, and products as a functional of the electron density. Thus, it has been successfully employed to understand the microscopic behavior of various physicochemical systems, and particularly to investigate the interaction energies at the interfaces.[31,32] We performed DFT calculations using the Vienna Ab-initio Software Package (VASP)[33] to simulate basic interactions between chemical species in the Na-MMT system with adequate simulation conditions for general chemical interaction. All calculations were carried out using the Perdew–Burke–Ernzerhof (PBE) exchange-correlation functional.[34] Electron–ion interactions were handled using the projector-augmented-wave (PAW) method for a plane wave with energy up to 500 eV. To model Na-MMT, we substituted one aluminum atom in the 2 × 2 pyrophyllite slab model with an oxygen-rich surface ($4Al_2(Si_4O_{10})(OH)_2$), with one magnesium atom; and included another sodium atom right on top of the oxygen layer, as shown in Figure S2 (Supporting Information). We then introduced an additional 15 Å vacuum layer along the *z*-axis. For the sampling of reciprocal space, we employed a 4 × 4 × 1 Monkhorst–Pack grid. A dipole correction was applied along the *z*-direction. The conjugate gradient algorithm using analytical forces, and the stress tensor, was chosen for the geometry-optimization method with 10^{-5} eV tolerances. All atomic positions at the mineral surface, as well as the adsorbents, were fully relaxed. To account for the solvation effect, we employed the Poisson–Boltzmann (PB) implicit-solvation model as implemented in the VASP program,[35] where the dielectric constant ε = 80 was used to describe water solvation (we neglected the contribution of cavitation energy).

Molecular Dynamics Simulation. Molecular dynamics (MD) simulation is useful to supplement experiments in interpreting observations and investigating dynamics from the atomistic level of understanding, and thus often utilized in studying hydrate formation dynamics.[28,36,37] In this study, the initial configurations of the 920 water, 30 CO_2, 6 zwitter-ionic glycine (Gly-zw), and a Na-MMT surface ($Na_{0.75}[Si_8](Al_{3.25}Mg_{0.75})O_{20}(OH)_4$)[38] used for the MD simulations are shown in Figure S3 (Supporting Information, the simulation cell size is 31.12 × 35.95 × 45.00 Å^3). The initial configuration of the Na-MMT surface structure was based on the DFT-minimized structure of pyrophyllite, and we randomly substituted 18 aluminum atoms with magnesium. In addition, 18 sodium atoms were randomly placed on the oxygen-rich mineral surface. Six glycine molecules were placed on the mineral surface for the glycine-adsorbed model. The interatomic potentials were described using the flexible 3-charge model (F3C) for water molecules,[39] the EPM2 model for CO_2 molecules,[40] the DREIDING force-field for glycine,[41] and the CLAYFF model for the Na-MMT.[42] To equilibrate the system, isobaric–isothermal ensemble (NPT) dynamics were performed for 2 ns at 273.15 K and 32 atm; only along the *z*-axis (surface normal direction) to equilibrate the simulation cell size, and then another 3 ns isothermal ensemble (NVT) dynamics was carried out to thermally equilibrate the system using the equilibrated cell parameters from the previous NPT simulation. We used the large-scale, atomic-modeling, massively parallelized simulation (LAMMPS) code.[43]

DOI: 10.1021/es504450x
Environ. Sci. Technol. 2015, 49, 1197–1205

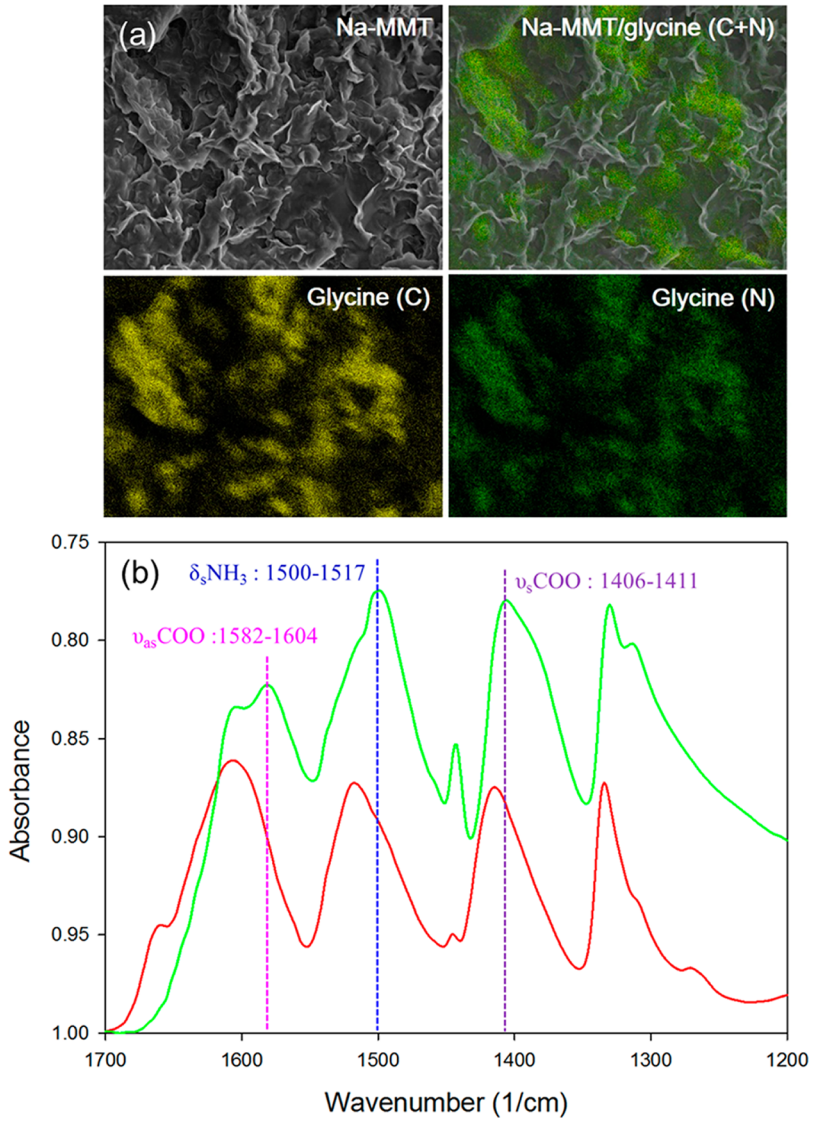

Figure 2. (a) SEM image of Na-MMT surface without glycine (Na-MMT). SEM/EDX mapping images of Na-MMT surface with glycine: carbon mapping image [Glycine (C)], nitrogen mapping image [Glycine (N)], and overlapping image [Na-MMT/glycine (C+N)] confirm that glycine molecules are evenly distributed on the surface of Na-MMT. (b) ATR-FTIR spectra of glycine solution (solid green line) and glycine complexed on Na-MMT surface (solid red line) at pH 8.32 ± 0.02. The blue dotted line is the symmetric deformation band of $-NH_3^+$ ($\delta_s NH_3$); the pink and violet dotted lines indicate the asymmetric stretch ($\upsilon_{as}COO$) and symmetric stretch ($\upsilon_s COO$), respectively.

RESULTS AND DISCUSSION

CO_2 Hydrate Induction Times. The formation kinetics of CO_2 hydrates involve the conventional nucleation-growth mechanism;[44] therefore, the nucleation stage is a metastable state where nuclei either grow or decompose. Spontaneous growth is usually observed after the nuclei exceed a critical size that depends on the surrounding environmental conditions. The time taken before spontaneous growth occurs (hydrate induction time) could provide an important index to CO_2 hydrate nucleation kinetics, which is known to follow log-normal distribution.[6]

Descriptive statistics, log-normal parameter estimates, and *p*-values for CO_2 hydrate induction time under different experimental conditions in DIW are described in Tables S3 and S4 (Supporting Information), respectively. Corresponding to statistical results under the four experimental conditions, specific *p*-values from the A-D and K-S tests exceeded 0.05 in all cases. This statistically confirms that distributions of CO_2 hydrate induction times for each condition can be properly characterized by log-normal probability density functions. Figure 1 shows relative-frequency histograms and variation of log-normal-fits of measured CO_2 hydrate induction times under different conditions in DIW. The *x*-and *y*-axes of the histograms show induction time and probability density, respectively, and are presented in different scales to demonstrate clearly the distribution patterns. We observed a decreasing shift in the arithmetic mean (μ_a) and SD (σ_a) of the log-normal distribution of CO_2 hydrate induction times in the order: D-G, DIW, D-M, and D-G-M. The μ_a and σ_a values of the D-G sample (97.97 ± 19.77 min) were 1.33 and 1.17 times greater than those for the DIW control (73.72 ± 16.85 min), whereas the values for D-M (41.20 ± 9.83 min) were 1.79 and 1.71 times smaller. This indicates that glycine plays the role of kinetic inhibitor, while Na-MMT plays a key role as kinetic promoter during CO_2 hydrate formation. These results are consistent with those of a previous study reporting that amino

DOI: 10.1021/es504450x
Environ. Sci. Technol. 2015, 49, 1197−1205

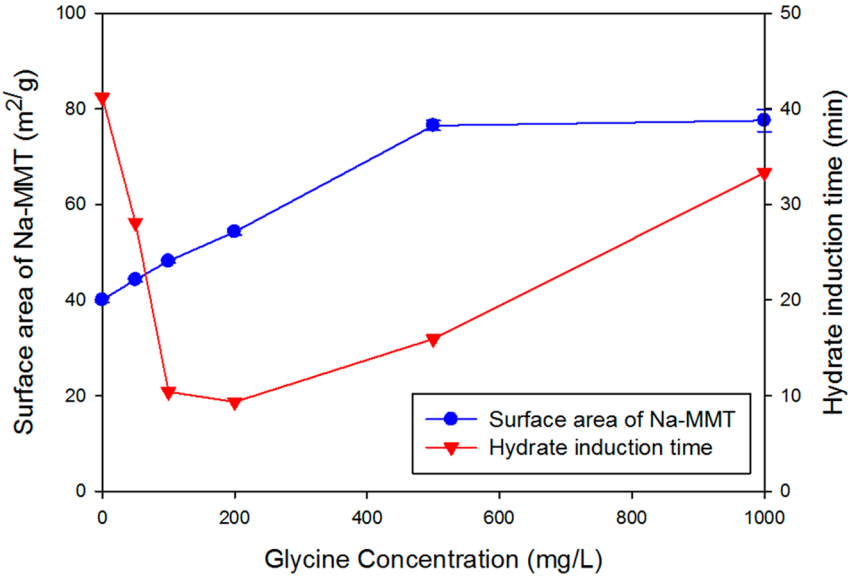

Figure 3. Variations of Na-MMT surface area (blue) and CO_2 hydrate induction time (red) at different glycine concentrations. Each hydrate induction time is arithmetic mean of log-normal distribution (μ_a) at each different glycine concentration (Table S6).

acids slow down hydrate nucleation kinetics due to perturbation of the organization of local water molecules, thus disrupting the hydrogen bond network of water.[45] It is also well-known that soil-mineral surfaces can provide nucleation sites that facilitate hydrate crystallization and act as stabilizers to prolong the lifetime of hydrate cages.[18,36] Interestingly, the sample containing both glycine and Na-MMT, showed considerably decreased CO_2 hydrate induction time (i.e., 7.08 times faster than the DIW control and 3.96 times faster than the D-M sample), with the smallest SD (10.41 ± 8.48 min). This indicates that the D-G-M sample provides the most favorable conditions to accelerate CO_2 hydrate nucleation kinetics by more consistently maintaining the hydrate-nucleation process. This result also implies that the potential interaction of glycine and Na-MMT could significantly enhance hydrate formation.

Evidence of Organo-Mineral Complexation. Because the dominant chemical species (>90%) of glycine in the D-G-M sample at pH 8.32 ± 0.02 is Gly-zw ($NH_3^+-CH_2-COO^-$: pK_{a1}, 2.34; pK_{a2}, 9.6),[24] the charged functional groups ($-NH_3^+$ and $-COO^-$) of Gly-zw are readily able to complex with surface oxygen and Na^+ cation, respectively, on Na-MMT surfaces.[46] A series of analyses using scanning electron microscopy with energy dispersive X-ray spectroscopy (SEM/EDX) and attenuated total reflectance Fourier-transform infrared spectroscopy (ATR-FTIR), verified the interaction between glycine and Na-MMT. The mapping image of carbon (yellow) and nitrogen (green) by EDX analysis (Figure 2a) confirms that glycine molecules were equally distributed on the Na-MMT surface. Figure 2b shows ATR-FTIR spectra of Gly-zw adsorbed on the Na-MMT surface (solid red line), and of the glycine solution (solid green line). A blue shift of each band provides direct evidence of an interaction between glycine and the Na-MMT surface. The shift in the symmetric deformation band of $-NH_3^+$ ($\delta_s NH_3$) from 1500 to 1517 cm^{-1} indicates a direct bond between the $-NH_3^+$ group and negatively charged oxygen atoms on the face of the Na-MMT via electrostatic attraction with hydrogen bonds.[24] In addition, blue shifts for asymmetric stretch ($\upsilon_{as}COO$, 1582−1604 cm^{-1}) and symmetric stretch ($\upsilon_s COO$, 1406−1411 cm^{-1}) indicate the presence of specific interactions of $-COO^-$ groups, with Na^+ near the mineral surface, as we can directly observe from the MD simulation in the next section.

Increase of Mineral−Water Interfacial Area. Considering that the enhanced hydrate nucleation kinetics involving soil minerals originated from the character of mineral−water interface, it is clear that the adsorption of glycine onto mineral surfaces alters their interfacial properties. First, we focused on the amount of interfacial area between the water and mineral surface. Figure 3 shows the variations of Na-MMT BET surface area (blue) and CO_2 hydrate induction time (red) at different glycine concentrations. In the presence of glycine, the surface area of Na-MMT was 1.11−1.94 times greater than that without glycine (40.04 ± 0.44 m^2/g). Although the BET measurement was carried out in a vacuum-dried condition, it is expected that the higher BET area of dried sample indicates the retention of the more dispersed state (with higher mineral−water interfacial area) of the aqueous suspension. As the concentration of glycine increased by 500 mg/L, the surface area of Na-MMT increased linearly; however, the surface was saturated as the glycine concentration further increased. This corresponded to results from a previous study reporting that sediment covered with a high concentration of organic matter could provide a greater surface area than that without organic matter.[7] Consequently, the more increased mineral−water interfacial area is able to provide the more hydrate-nucleation sites to interact well with the surrounding hydrate-forming molecules. Based on the classical nucleation theory, more nucleation sites increases the rate of nucleation, leading to faster hydrate formation.[18,28,47]

According to the QM energetics, the binding of Gly-zw to the mineral surface by coordination between $-NH_3^+$ groups and surface oxygen atoms, was very stable (24.6 kcal/mol). In addition, we found that the stabilization energy due to the water solvation (normalized by the surface-area) of the Gly-zw-covered surface (30.5 kcal/mol•nm^2) was 1.45 times greater than that of a bare mineral surface (21.0 kcal/mol•nm^2). This is due to the enhanced polarity of the surface originating from the ionic functional groups of Gly-zw with strong polarity, which effectively stabilizes the mineral surface in aqueous

DOI: 10.1021/es504450x
Environ. Sci. Technol. 2015, 49, 1197−1205

solution. Similar to the role of surfactants in stabilizing nanoparticles in solution and forming an emulsion state,[48] it is expected that the surface-adsorbed Gly-zw will help stabilize the suspended state of mineral in aqueous solution.

However, it should be noted that the nucleation kinetics of CO_2 hydrate was maximally enhanced (9.35 ± 6.52 min) at 200 mg/L of glycine concentration (Tables S5 and S6, Supporting Information) and retarded by almost no glycine, although the change in surface area showed a monotonic increase and saturation behavior. The amount of glycine at the mineral–water interface is saturated at 200 mg/L concentration (see the Supporting Information). Thus, the excessive glycine (over 200 mg/L) is apt to be dissolved in the aqueous phase and subsequently act as an inhibitor of hydrate formation. This reasonably explains the retarded nucleation kinetics of CO_2 hydrate when the glycine concentration exceeds 200 mg/L.

Changes of the Mineral–Water Interfacial Characteristics. The maximally enhanced hydrate induction time with the D-G-M sample was approximately 4 times faster than that of the D-M sample. This indicates that the change of nucleation kinetics is attributed to the change of the characteristics of the mineral–water interface, as well as the area of the mineral–water interface. To grasp an atomistic level of understanding of the organo-mineral complex interfacial characteristics, we performed MD simulations of a system close to the experimental conditions. Figure 4 shows comparisons of the spatial distributions of water, CO_2, and Na^+ along the direction normal to the Na-MMT surface (chosen as z-direction), averaged from 3 ns NVT MD trajectories. The local density of water and CO_2 at the mineral surface was very high due to the interaction of water and CO_2 with the polar Na-MMT surface. Sharp peaks formed in the close vicinity of the mineral surface as a discrete shell (Figure 4a,b). It has been reported that the high local density of hydrate-forming molecules are apparently a critical factor in inducing nucleation.[49−51] This suggests that the nucleation rate might be enhanced near the mineral surface, which would explain the enhanced CO_2 hydrate nucleation kinetics of D-M and D-G-M.

Although there was a marginal change in the water and CO_2 distribution with respect to the presence of glycine, we found that the Na^+ distribution was evidently changed by glycine. The Na^+ ions are mainly located between the first and second water layers from the mineral surface, and surrounded by water molecules forming a strong solvation shell. However, in the case of glycine molecules adsorbed to the mineral surface, the population of Na^+ in the first shell decreased while that in the second shell increased (Figure 4c). This is due to the negatively charged $-COO^-$ group of Gly-zw, which is strongly coordinated with Na^+ from the mineral surface.

Radial-distribution function analysis of Na^+ from oxygen on the $-COO^-$ functional group of glycine is shown in Figure 5a. The number of Na^+ atoms in the first coordination shell was 0.5, indicating that each COO^- group was strongly coordinated with one Na^+ ion, on average. This explains the experimental observation of the blue-shift of vibrational COO^- peaks using measurements with ATR-FTIR spectroscopy. From these observations, we would expect that the thermal motions of solvated Na^+ on mineral surfaces would be quenched by coordination with glycine. The diffusion coefficients of Na^+ of D-M and D-G-M systems are shown in Figure 5b. The coefficient of the D-G-M system (2.00×10^{-5} cm^2/s) was almost half that of the D-G system (3.93×10^{-5} cm^2/s). This supports that Na^+ ions are effectively immobilized by surface

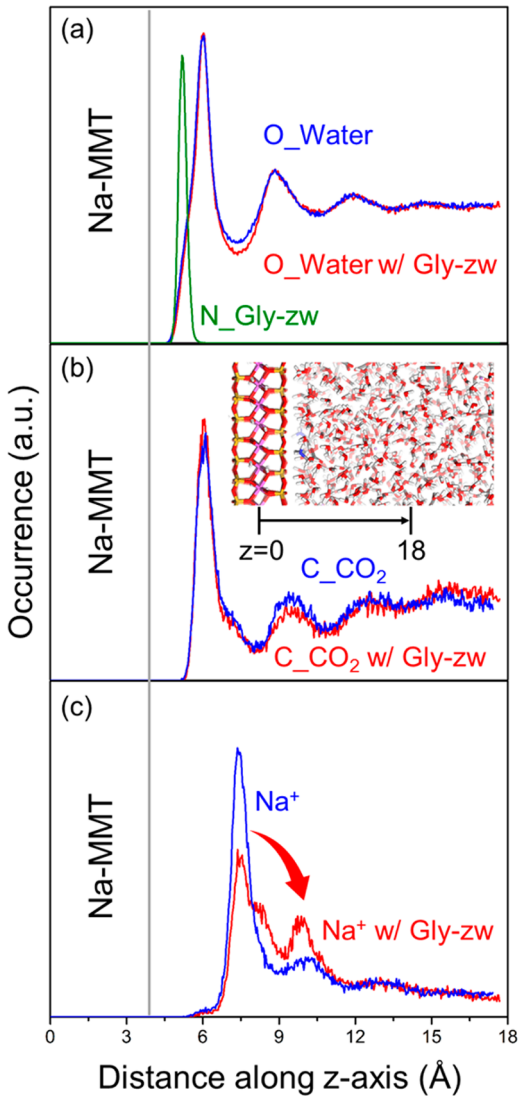

Figure 4. Distribution of major components: (a) glycine and water, (b) CO_2, and (c) Na^+ computed from 3 ns MD simulation. The z-axis was chosen as the surface normal direction. The local density of water and CO_2 near the mineral surface is markedly higher than in the bulk. Na^+ in the first shell (near the mineral surface) is displaced into the second shell when glycine is added to the system.

glycine in a D-G-M system. Considering that the thermal motion of Na^+ in the vicinity of a mineral surface has an inhibiting effect on hydrate nucleation kinetics by disrupting the hydrogen-bonded water-molecule network,[18,52] the adsorption of glycine to the Na-MMT surface would effectively enhance hydrate nucleation kinetics by decreasing the thermal fluctuation of Na^+ at the mineral surface. However, glycine molecules dissolved in the aqueous phase retard the hydrate nucleation kinetics (as shown in the D-G system) due to the zwitter-ionic functional groups disturbing the hydrogen-bond networks of water molecules.

Effect of Organo–Mineral Complex in High Salinity Condition. The effect of an organo-mineral complex on CO_2 hydrate nucleation kinetics was also investigated at high salinity (3.5% w/w NaCl solution) to evaluate its applicability to offshore CO_2 sequestration in marine sediments (Figure S4, and Tables S7 and S8, Supporting Information). The μ_a and σ_a values of the N-M sample (28.31 ± 7.08 min) were 1.46 and

DOI: 10.1021/es504450x
Environ. Sci. Technol. 2015, 49, 1197−1205

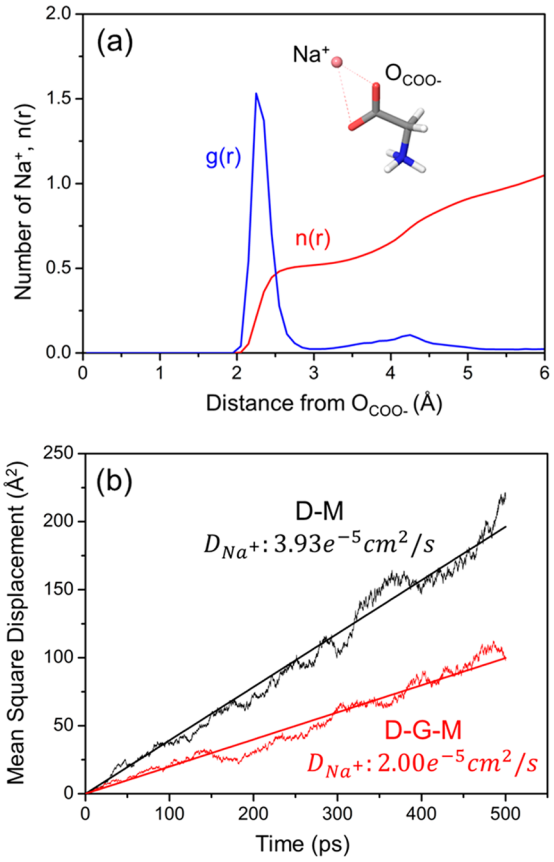

Figure 5. (a) Radial distribution function analysis of Na^+ from oxygen on the $-COO^-$ functional group of glycine. (b) Diffusion coefficients of Na^+ for D-M and D-G-M system.

1.39 times smaller than those for the D-M sample (41.20 ± 9.83 min). This indicates that the promoting effect of Na-MMT surface on CO_2 hydrate formation could be further enhanced in the presence of electrolytes. It is known that electrolytes can inhibit hydrate nucleation in aqueous solution by association with water molecules, thus reducing the activity of water.[7,18,52] On the other hand, a high concentration of electrolyte (NaCl) could help build more sophisticated mineral structures (Na-MMT), providing more suitable hydrate nucleation sites, due to the formation of compressed electric double layers via strong adsorption of cation (Na^+) on the mineral face site.[6] The structural change of Na-MMT providing more facilitative surface nucleation sites, could overwhelm the inhibition effect by electrolytes, resulting in enhanced nucleation kinetics of CO_2 hydrate. The CO_2 hydrate induction times of the N-G-M sample (17.49 ± 4.85 min) were 1.62 times faster than those of the N-M sample (28.31 ± 7.08 min) and 1.68 times slower than those of the D-G-M sample (10.41 ± 8.48 min). This indicates that the potential role of the organo-mineral complex as a hydrate nucleation promoter would be influential even at high salinity, although its effect might be a bit less than that in DIW. This implies that the nucleation kinetics of CO_2 hydrate could be significantly enhanced by the interaction of organic matter and sediment minerals during offshore CO_2 sequestration in real marine sediment environments.

Environmental Implications for CO_2 Sequestration. Adsorption of organic matter onto sediment-mineral surfaces is an important process in natural environments.[22−24] This can lead to formation of organo-mineral complexes, potentially affecting hydrate formation kinetics (kinetics of nucleation and growth) during the offshore CO_2 sequestration under seabed sediments. Research has shown the characteristics and role of organo-mineral complexes (formed via adsorption of Gly-zw onto the Na-MMT surface), on CO_2 hydrate nucleation kinetics. We observed enhanced CO_2 hydrate nucleation kinetics in the presence of an organo-mineral complex. The electrostatic interaction between the zwitter-ionic organic molecule of glycine, and the mineral surface, forms an organo-mineral complex that provides increased mineral−water interfacial area for CO_2 hydrate nucleation. The zwitter-ionic character also plays the additional significant role of quenching the thermal motion of Na^+ (a kinetic inhibitor). This increases the probability of hydrate nucleation at the mineral−water interface, and enhances the hydrate nucleation kinetics. This also implies that marine environmental factors in local CO_2 storage sites, and their interactions, might significantly vary the probability distribution of CO_2 hydrate induction times. Therefore, understanding the characteristics of hydrate formation within heterogeneous marine environmental systems is necessary for successful implementation of offshore CO_2 sequestration technology.

The formation of CO_2 hydrate, and the development of a hydrate cap over real seabed sediments, could be influenced by heterogeneity of the marine environment (e.g., variation in the types and quantities of soil minerals and organic matter). Further understanding of these diverse factors and their interactions may contribute to making better choices about where to store, and how to sequester, CO_2 by hydrate formation. The experimental and computational results obtained from this study may not provide a full understanding of offshore CO_2 storage in actual marine sediment environments. Nonetheless, they may deliver new insights into the proper selection of CO_2 storage sites, their suitable design and optimal operation, and prevention of CO_2 leakage from them. Furthermore, these insights could also provide useful guidelines and tactics for the development of novel offshore CO_2 sequestration technology, and for its successful implementation in the near future.

■ ASSOCIATED CONTENT

Supporting Information

Analytical procedures including SEM/EDX, ATR/FTIR, and surface analysis (BET), order estimation of glycine adsorption, schematic of experimental setup, quantum mechanical and molecular dynamics structures, stochastic data set, descriptive statistics, and log-normal parameter estimates and *p*-values for CO_2 hydrate induction time under different experimental conditions. This material is available free of charge via the Internet at http://pubs.acs.org.

■ AUTHOR INFORMATION

Corresponding Author

*W. Lee. Phone: +82-42-350-3624. Fax: +82-42-350-3610. E-mail: woojin_lee@kaist.ac.kr.

Notes

The authors declare no competing financial interest.

■ ACKNOWLEDGMENTS

This work was financially supported by research grants from the National Research Foundation of Korea funded by the Korean Government (MEST) (Grant No. NRF-2012-C1AAA001-

DOI: 10.1021/es504450x
Environ. Sci. Technol. 2015, 49, 1197−1205

M1A2A2026588), Global Frontier R&D Program (2013M3A6B1078884) on Center for Hybrid Interface Materials (HIM) funded by the Ministry of Science, ICT, and Future Planning of the Korean Government, and High-tech Urban Development Program funded by the Ministry of Land, Infrastructure and Transport of the Korean Government (11 High Tech G08).

REFERENCES

(1) Sloan, E. D. Fundamental principles and applications of natural gas hydrates. *Nature* **2003**, *426*, 353−363.
(2) Takeya, S.; Ripmeester, J. A. Dissociation behavior of clathrate hydrates to ice and dependence on guest molecules. *Angew. Chem., Int. Ed.* **2008**, *47*, 1276−1279.
(3) Wright, J. F.; Côté, M. M.; Dallimore, S. R. Overview of regional opportunities for geological sequestration of CO_2 as gas hydrate in Canada. *6th International Conference on Gas Hydrates (ICGH) 2008*, Vancouver, BC, Canada, July 6−10, 2008.
(4) Zatsepina, O. Y.; Pooladi-Darvish, M. Storage of CO_2 hydrate in shallow gas reservoirs: Pre- and post-injection periods. *Greenhouse Gas Sci. Technol.* **2011**, *1*, 223−236.
(5) Lamorena, R. B.; Kyung, D.; Lee, W. Effect of organic matters on CO_2 hydrate formation in Ulleung Basin sediment suspensions. *Environ. Sci. Technol.* **2011**, *45*, 6196−6203.
(6) Lee, K.; Lee, S.; Lee, W. Stochastic nature of carbon dioxide hydrate induction times in Na-montmorillonite and marine sediment suspensions. *Int. J. Greenhouse Gas Control* **2013**, *14*, 15−24.
(7) Kyung, D.; Lee, K.; Kim, H.; Lee, W. Effect of marine environmental factors on the phase equilibrium of CO_2 hydrate. *Int. J. Greenhouse Gas Control* **2014**, *20*, 285−292.
(8) Rehder, G.; Kirby, S. H.; Durham, W. B.; Stern, L. A.; Peltzer, E. T.; Pinkston, J.; Brewer, P. G. Dissolution rates of pure methane hydrate and carbon-dioxide hydrate in undersaturated seawater at 1000-m depth. *Geochim. Cosmochim. Acta* **2004**, *68*, 285−292.
(9) Lapham, L. L.; Wilson, R. M.; MacDonald, I. R.; Chanton, J. P. Gas hydrate dissolution rates quantified with laboratory and seafloor experiments. *Geochim. Cosmochim. Acta* **2014**, *125*, 492−503.
(10) Lee, S.; Liang, L.; Riestenberg, D.; West, O. R.; Tsouris, C.; Adams, E. CO_2 hydrate composite for ocean carbon sequestration. *Environ. Sci. Technol.* **2003**, *37*, 3701−3708.
(11) House, K. Z.; Schrag, D. P.; Harvey, C. F.; Lackner, K. S. Permanent carbon dioxide storage in deep-sea sediments. *Proc. Natl. Acad. Sci. U. S. A.* **2006**, *103*, 12291−12295.
(12) Tohidi, B.; Yang, J.; Salehabadi, M.; Anderson, R.; Chapoy, A. CO_2 hydrates could provide secondary safety factor in subsurface sequestration of CO_2. *Environ. Sci. Technol.* **2010**, *44*, 1509−1514.
(13) Lee, H.; Seo, Y.; Seo, Y.-T.; Moudrakovski, I. L.; Ripmeester, J. A. Recovering methane from solid methane hydrate with carbon dioxide. *Angew. Chem., Int. Ed.* **2003**, *42*, 5048−5051.
(14) Park, Y.; Kim, D.-Y.; Lee, J.-W.; Huh, D.-G.; Park, K.-P.; Lee, J.; Lee, H. Sequestering carbon dioxide into complex structures of naturally occurring gas hydrates. *Proc. Natl. Acad. Sci. U. S. A.* **2006**, *103*, 12690−12694.
(15) Espinoza, D. N.; Santamarina, J. C. P-wave monitoring of hydrate-bearing sand during CH_4-CO_2 replacement. *Int. J. Greenhouse Gas Control* **2011**, *5*, 1031−1038.
(16) Teng, H.; Yamasaki, A.; Shindo, Y. The fate of CO_2 hydrate released in the ocean. *Int. J. Energy Res.* **1999**, *23*, 295−302.
(17) Warzinski, R. P.; Lynn, R. J.; Haljasmaa, I.; Zhang, Y.; Holder, G. D. Dissolution of CO_2 drops and CO_2 hydrate stability under simulated deep ocean conditions in a high-pressure water tunnel. *3rd Annual Conference on Carbon Sequestration*, Alexandria, Virginia, May 3−6, 2004.
(18) Lamorena, R. B.; Lee, W. Formation of carbon dioxide hydrate in soil and soil mineral suspensions with electrolytes. *Environ. Sci. Technol.* **2008**, *42*, 2753−2759.
(19) Lamorena, R. B.; Lee, W. Effect of pH on carbon dioxide hydrate formation in mixed soil mineral suspensions. *Environ. Sci. Technol.* **2009**, *43*, 5908−5914.
(20) Lim, L. H. V.; Lloren, A. V.; Lamorena, R. B. The effect of urea in the nucleation process of CO_2 clathrate hydrates. *J. Mol. Liq.* **2014**, *194*, 245−250.
(21) Park, T.; Kyung, D.; Lee, W. Effect of organic matter on CO_2 hydrate phase equilibrium in phyllosilicate suspensions. *Environ. Sci. Technol.* **2014**, *48*, 6597−6603.
(22) Hedges, J. I.; Hare, P. E. Amino acid adsorption by clay minerals in distilled water. *Geochim. Cosmochim. Acta* **1987**, *51*, 255−259.
(23) Kawahata, H.; Ishizuka, T. Amino acids in the sediments and interstitial waters from ODP holes 677B and 678B in the Panama basin. *Oceanol. Acta* **1993**, *16*, 373−379.
(24) Ramos, M. E.; Huertas, F. J. Adsorption of glycine on montmorillonite in aqueous solutions. *Appl. Clay Sci.* **2013**, *80*−*81*, 10−17.
(25) Shroll, R. M.; Smith, D. E. Molecular dynamics simulations in the grand canonical ensemble: application to clay mineral swelling. *J. Chem. Phys.* **1999**, *111*, 9025−9033.
(26) Yoon, T. H.; Johnson, S. B.; Musgrave, C. B.; Brown, G. E., Jr. Adsorption of organic matter at mineral/water interfaces: I. ATR-FTIR spectroscopic and quantum chemical study of oxalate adsorbed at boehmite and corundum/water interfaces. *Geochim. Cosmochim. Acta* **2004**, *68*, 4505−4518.
(27) Wang, J.; Kalinichev, A. G.; Kirkpatrick, R. J. Effect of substrate structure and composition on the structure, dynamics, and energetics of water at mineral surfaces: A molecular dynamics modeling study. *Geochim. Cosmochim. Acta* **2006**, *70*, 562−582.
(28) Bai, D.; Chen, G.; Zhang, X.; Wang, W. Microsecond molecular dynamics simulations of the kinetic pathways of gas hydrate formation from solid surfaces. *Langmuir* **2011**, *27*, 5961−5967.
(29) Kastner, M. Oceanic minerals: Their origin, nature of their environment, and significance. *Proc. Natl. Acad. Sci. U. S. A.* **1999**, *96*, 3380−3387.
(30) Guo, G. J.; Zhang, Y. G.; Refson, K. Effect of H-bond topology on the lifetimes of cagelike water clusters immersed in liquid water and the probability distribution of these lifetimes: Implications for hydrate nucleation mechanisms. *Chem. Phys. Lett.* **2005**, *413*, 415−419.
(31) Jeon, S.; Kim, H.; Goddard, W. A.; Atwater, H. A. DFT study of water adsorption and decomposition on a Ga-Rich GaP(001)(2×4) surface. *J. Phys. Chem. C* **2012**, *116*, 17604−17612.
(32) Shin, H.; Jung, S.; Bae, S.; Lee, W.; Kim, H. Nitrate reduction mechanism on a Pd surface. *Environ. Sci. Technol.* **2014**, *48*, 12768−12774.
(33) Kresse, G.; Furthmüller, J. Efficient iterative schemes for *ab initio* total-energy calculations using a plane-wave basis set. *J. Phys. Rev. B* **1996**, *54*, 11169.
(34) Perdew, J. P.; Burke, K.; Ernzerhof, M. Generalized gradient approximation made simple. *Phys. Rev. Lett.* **1996**, *77*, 3865.
(35) Fishman, M.; Zhuang, H. L.; Mathew, K.; Dirschka, W.; Hennig, R. G. Accuracy of exchange-correlation functionals and effect of solvation on the surface energy of copper. *Phys. Rev. B* **2013**, *87*, 245402.
(36) Bai, D.; Chen, G.; Zhang, X.; Wang, W. Nucleation of the CO_2 hydrate from three-phase contact lines. *Langmuir* **2012**, *28*, 7730−7736.
(37) Walsh, M. R.; Koh, C. A.; Sloan, E. D.; Sum, A. K.; Wu, D. T. Microsecond simulations of spontaneous methane hydrate nucleation and growth. *Science* **2009**, *326*, 1095−1098.
(38) Whitley, H. D.; Smith, D. E. Free energy, energy, and entropy of swelling in Cs-, Na-, and Sr-montmorillonite clays. *J. Chem. Phys.* **2004**, *120*, 5387−5395.
(39) Levitt, M.; Hirshberg, M.; Sharon, R.; Laidig, K. E.; Daggett, V. Calibration and testing of a water model for simulation of the molecular dynamics of proteins and nucleic acids in solution. *J. Phys. Chem. B* **1997**, *101*, 5051−5061.

DOI: 10.1021/es504450x
Environ. Sci. Technol. 2015, 49, 1197−1205

(40) Harris, J. G.; Yung, K. H. Carbon dioxide's liquid-vapor coexistence curve and critical properties as predicted by a simple molecular model. *J. Phys. Chem.* **1995**, *99*, 12021−12024.
(41) Mayo, S. L.; Olafson, B. D.; Goddard, W. A. DREIDING: A generic force field for molecular simulations. *J. Phys. Chem.* **1990**, *94*, 8897−8909.
(42) Cygan, R. T.; Liang, J.-J.; Kalinichev, A. G. Molecular models of hydroxide, oxyhydroxide, and clay phases and the development of a general force field. *J. Phys. Chem. B* **2004**, *108*, 1255−1266.
(43) Plimpton, S. Fast parallel algorithms for short-range molecular dynamics. *J. Comput. Phys.* **1995**, *117*, 1−19.
(44) Sloan, E. D.; Koh, C. A. *Clathrate Hydrates of Natural Gases*, 3rd ed.; CRC Press, Taylor and Francis Group: Boca Raton, FL, 2008.
(45) Sa, J.-H.; Kwak, G.-H.; Lee, B. R.; Park, D.-H.; Han, K.; Lee, K.-H. Hydrophobic amino acids as a new class of kinetic inhibitors for gas hydrate formation. *Sci. Rep.* **2013**, *3*, 2428.
(46) Pareek, A.; Torrelles, X.; Angermund, K.; Rius, J.; Magdans, U.; Gies, H. Competitive adsorption of glycine and water on the fluorapatite (100) surface. *Langmuir* **2009**, *25*, 1453−1458.
(47) Park, S.-H.; Sposito, G. Do montmorillonite surfaces promote methane hydrate formation? Monte Carlo and molecular dynamics simulations. *J. Phys. Chem. B* **2003**, *107*, 2281−2290.
(48) Bibette, J.; Leal-Calderon, F. Surfactant-stabilized emulsions. *Curr. Opin. Colloid Interface Sci.* **1996**, *1*, 746−751.
(49) Vatamanu, J.; Kusalik, P. G. Observation of two-step nucleation in methane hydrates. *Phys. Chem. Chem. Phys.* **2010**, *12*, 15065−15072.
(50) Sarupria, S.; Debenedetti, P. G. Homogeneous nucleation of methane hydrate in microsecond molecular dynamics simulations. *J. Phys. Chem. Lett.* **2012**, *3*, 2942−2947.
(51) Pirzadeh, P.; Kusalik, P. G. Molecular insights into clathrate hydrate nucleation at an ice-solution interface. *J. Am. Chem. Soc.* **2013**, *135*, 7278−7287.
(52) Dholabhai, P. D.; Kalogerakis, N.; Bishnoi, P. R. Kinetics of methane hydrate formation in aqueous electrolytes solutions. *Can. J. Chem. Eng.* **1993**, *71*, 68−74.

DOI: 10.1021/es504450x
Environ. Sci. Technol. 2015, 49, 1197−1205